HIGH-Q REFLECTION NOTCH METHOD FOR MM WAVE MEASUREMENTS OF LARGE DIELECTRIC LOSSES USING A STACK RESONATOR: ANALYSIS AND SIMULATIONS

V. B. Yurchenko[*]

Usikov Institute of Radiophysics and Electronics, National Academy of Sciences of Ukraine, 12, Proskura St., Kharkov 61085, Ukraine

Abstract—A high-Q reflection notch method for measuring large dielectric losses in absorbing materials when using a stack resonator, which is a one-dimensional analogue of a capillary-in-a-waveguide technique, has been proposed. A detailed explanation of the effects that lay the basis of the method has been presented. The method is particularly accurate and sensitive for highly absorbing materials when other techniques are inadequate. The method can be used for dielectric spectroscopy of a broad range of liquid and solid materials, with applications in chemical, pharmaceutical and food industry, biomedical sciences, agriculture etc., in those frequency bands of infrared, millimeter wave and, especially, THz waves where dielectric losses are significant.

1. INTRODUCTION

For measuring high-frequency dielectric losses, there are many experimental methods [1–11], of which resonant techniques are particularly attractive and beneficial [5–11]. Of various techniques, there is one interesting method based on observing high-quality transmission notches (of quality factor $Q \sim 300$–500) in a system of highly absorbing liquid (of loss tangent $\tan(\delta) > 1$) confined in a capillary which is mounted in a waveguide [12–16]. The method is found to be excellent for measuring high-frequency dielectric parameters of highly absorbing liquids, e.g., water solutions of complex permittivity $\epsilon = \epsilon_r + i\epsilon_i$ with typical values $\epsilon_r \sim 10$–30 and $\epsilon_i \sim 20$–40 at millimeter waves. Advantages of the method include high accuracy

and sensitivity of the technique, simplicity of implementation, small quantity of liquid required, etc. As a result, numerous applications of the method exist, particularly, in chemical, pharmaceutical and food industry, biomedical sciences, and so on.

Despite the fact that the method is known for more than 20 years, the physics behind the technique is not completely clear [12–16]. The most intriguing feature of the effect is the growth of the quality factor Q of the transmission notch with increasing the loss tangent $\tan(\delta) = \epsilon_i/\epsilon_r$ in the domain of parameters being considered (when ϵ_i increases due to increase of electrical conductivity σ where $\epsilon_i = \sigma/\omega\epsilon_0$ in the SI units, ϵ_0 is the absolute dielectric constant of vacuum, $\omega = 2\pi f$ is the angular frequency, and f is the frequency of the incident wave).

Known attempts of theoretical analysis of the effect [12–16] are incomplete and unsatisfactory (no direct proofs were actually presented that either the excitation of surface waves or resonant absorption does, really, create a high-Q transmission notch), except the paper [17] that provides an explanation in terms of interference effects, though, unfortunately, with no analysis of absorption (therefore, with no answer whether any high-Q resonant absorption occurs in the process or not). The reason for such a controversial situation is, probably, a relative complexity of a real system (a cylindrical capillary cuvette with highly absorbing liquid mounted as an inductive rod in a rectangular waveguide) that was not properly represented in any simplified model.

The aim of this paper is to propose, theoretically analyze, and numerically simulate an alternative measurement system — a special kind of one-dimensional stack resonator — where the same sort of effects would take place (though, in this case, in reflection) so as the effects could be explained in full detail and, on this basis, an enhanced high-Q resonant method could be developed for dielectric measurements of a broad range of liquid and solid materials in those frequency bands of infrared, millimeter wave and, especially, THz waves where dielectric losses are significant.

2. A MODEL OF THE MEASUREMENT CELL

We consider a model measurement cell made of an open one-dimensional stack (Bragg) resonator that consists of four dielectric plates and a layer of absorbing liquid confined between the inner plates as shown in Figure 1 (a dark area in the middle shows the layer of liquid, four gray strips represent dielectric plates, and white areas between plates show the air slots).

A weakly resonant cell as needed for the effects to appear is
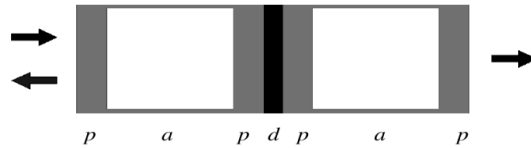
Figure 1. A measurement cell made of a four-plate stack (Bragg) resonator with a layer of lossy liquid confined between the inner plates (d is the layer of liquid, p is the plastic plate, a is the air slot, and the arrows show the incident, reflected and transmitted waves).

made of polycarbonate plates of thickness $p = 0.85$ mm with air slots $a = 3.5$ mm and a liquid layer $d = 0.5$ mm. The plates are characterized by complex permittivity $\epsilon_p = \epsilon_{pr} + i\epsilon_{pi}$ where $\epsilon_{pr} = 3$, $\epsilon_{pi} = \sigma_p/\omega\epsilon_0$, $\sigma_p = 0.15$ Sm/m (loss tangent $\tan(\delta) = 0.015$ at $f = 60$ GHz) and the liquid is described by the model permittivity $\epsilon = \epsilon_r + i\epsilon_i$ where $\epsilon_r = 16$, $\epsilon_i = \sigma/\omega\epsilon_0$ and σ is, typically, chosen in the range of $\sigma = 0 - 100$ Sm/m (e.g., $\tan(\delta) = 1.1$ and $\epsilon_i = 18$ at $f = 60$ GHz and $\sigma = 60$ Sm/m). The latter values were chosen so as to represent a typical case of water, once the real and imaginary parts of water permittivity $\epsilon_w(\omega)$ vary in the range $\epsilon_{wr} = 27 - 9$ and $\epsilon_{wi} = 36 - 17$ in the frequency band $f = 30 - 90$ GHz, respectively ($\epsilon_{wr} = 12$ and $\epsilon_{wi} = 23$ at $f = 60$ GHz) [18, 19].

Assuming a uniform plane wave of linear polarization propagating along the z- axis and incident on the stack from the left side, we can easily obtain (by utilizing, e.g., a transmission matrix method [20]) an exact solution for the field distribution in the stack and for the complex scattering matrix coefficients S_{11} and S_{21} (here, $S_{12} = S_{21}$ and, due to the stack symmetry, $S_{22} = S_{11}$). Then we can easily compute both the parametric and frequency dependencies of any quantity, including the transmission power $P_{tr} = |S_{21}|^2$, reflection power $P_{ref} = |S_{11}|^2$, and absorption power $P_{abs} = 1 - (P_{tr} + P_{ref})$.

Basic implementation of the measurement method (similar to [12–16]) consists in measuring the reflection power P_{ref} as a function of frequency f for the liquid of unknown ϵ_r and ϵ_i assuming both the stack geometry and the complex permittivity of plates are known. Then, by comparing measurements with simulations, we could recover both the real and imaginary parts of complex permittivity of liquid. Other ways of parameter extraction are possible, e.g., by evaluating the reflection notch frequency f_n and the notch quality factor Q_n from the measured data and comparing them with a set of reference values, etc.

Now, consider the effects emerging in the structure under the mm-wave excitation.

3. REFLECTION, TRANSMISSION, AND ABSORPTION SPECTRA

Basic effects are illustrated in Figure 2 that shows the mm-wave reflection, transmission, and absorption spectra of the measurement cell filled with dielectric liquid of complex permittivity $\epsilon(\omega) = \epsilon_r + i\epsilon_i(\omega)$. The real part of liquid permittivity is assumed to be constant and equal to $\epsilon_r = 16$ while the imaginary part $\epsilon_i(\omega)$ is linked with the electric conductivity by the relation $\epsilon_i(\omega) = \sigma/\omega\epsilon_0$. Bold and thin curves are computed for the liquid conductivity $\sigma = 60\,\mathrm{Sm/m}$ and $90\,\mathrm{Sm/m}$, respectively. Other parameters are chosen to be $d = 0.5\,\mathrm{mm}$, $a = 3.5\,\mathrm{mm}$, $p = 0.85\,\mathrm{mm}$, $\epsilon_{pr} = 3$, and $\sigma = 0.15\,\mathrm{Sm/m}$ as explained above.

The main effect is that the second reflection notch observed at the frequency $f_2 = 56\,\mathrm{GHz}$ is going deeper and the notch quality factor Q_2 (defined by the notch full width Δf at half depth as $Q_n = f_n/\Delta f$ where f_n is the n-th notch frequency) increases with increasing the dielectric losses when liquid conductivity grows from $\sigma = 60\,\mathrm{Sm/m}$ to nearly $130\,\mathrm{Sm/m}$ (the loss tangent $\tan(\delta)$ increases from 1.2 to 2.6 while the imaginary part of ϵ grows from $\epsilon_i = 19$ to $\epsilon_i = 42$). Similar effect is observed at the first notch frequency $f_1 = 33\,\mathrm{GHz}$, though it occurs at $\sigma < 30\,\mathrm{Sm/m}$ where $\tan(\delta) < 1$ and $\epsilon_i < 16$ (exact values of f_n depend slightly on liquid conductivity σ).

Computed values of Q_2 are found to be 14 at $\sigma = 60\,\mathrm{Sm/m}$
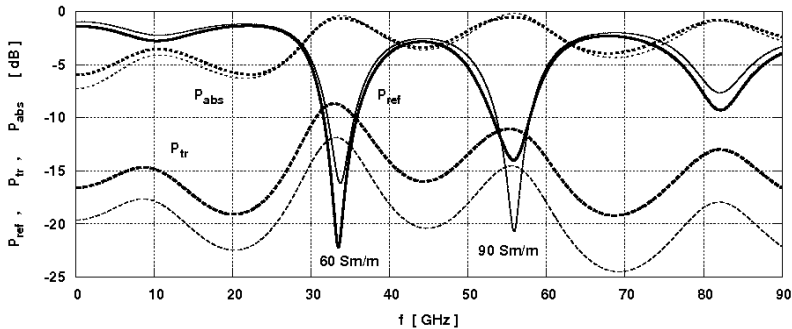
Figure 2. Reflection P_{ref}, transmission P_{tr}, and absorption P_{abs} power spectra of measurement cell of Figure 1 with liquid of permittivity $\epsilon(\omega) = \epsilon_r + i\sigma/\omega\epsilon_0$ at $\sigma = 60\,\mathrm{Sm/m}$ and $\sigma = 90\,\mathrm{Sm/m}$ (bold and thin curves, respectively) when $\epsilon_r = 16$, $d = 0.5\,\mathrm{mm}$, $a = 3.5\,\mathrm{mm}$, $p = 0.85\,\mathrm{mm}$, $\epsilon_{pr} = 3$, and $\sigma_p = 0.15\,\mathrm{Sm/m}$.

($P_{ref} = -14$ dB), about 45 at $\sigma = 90$ Sm/m ($P_{ref} = -20$ dB), and nearly 1400 at $\sigma = 130$ Sm/m ($P_{ref} = -49$ dB), though measured values would be limited by imperfections of the measurement system (e.g., the source frequency instability $\delta f \sim 0.1$ GHz would limit the notch quality factor at the level of $f/\delta f \sim 300$–500 at the frequencies $f = 30$ GHz and 50 GHz, respectively).

The reflection notch frequencies correspond to certain resonant effects in the cell structure. At these frequencies, broad maxima of nearly complete absorption appear and equally broad maxima of transmission also emerge, though at a low level because of strong absorption. The absorption and transmission maxima at the frequency f_2 and conductivity values specified above are characterized by quality factors 3, 3.5, 4.3 and 5, 6.1, 8.0, respectively, that is much lower than the reflection notch quality factors Q_n.

The fact that the reflection notch quality factors Q_n are so high at large absorption and so sensitive to conductivity variations allows one to use the effect for the accurate measurements of large dielectric losses in absorbing materials, similarly to the transmission notch effect in a capillary system [12–16].

4. FIELDS AND POWER FLUXES IN THE CELL

Once having a complete solution, one can obtain spatial distributions of the wave fields and power fluxes across the cell. Figures 3 and 4 show the fields and power fluxes computed at the frequency $f = 33.5$ GHz close to the first branch-point (see below) reflection notch frequency
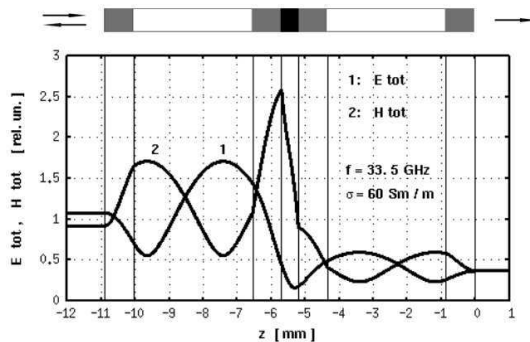
Figure 3. Total electric (E_{tot}) and magnetic (H_{tot}) fields in the cell of Figure 1 at the frequency $f = 33.5$ GHz close to the first branch-point frequency $f_{01} = 33.00$ GHz when $\sigma = 60$ Sm/m (inset above shows the measurement cell).

$f_{01} = 33.00\,\text{GHz}$ for the cell of Figure 1 when $\sigma = 60\,\text{Sm/m}$.

The results show that the resonant effects develop, mainly, in the front part of the cell structure whereas absorption occurs, mostly, in the liquid layer. Similar effects are observed near the second branch-point frequency $f_{02} = 56.02\,\text{GHz}$ and even, to a certain extent, at the intermediate frequencies like $f = 45\,\text{GHz}$, though, in the latter case, standing waves are smaller and the reflection power is greater.

The effects look similar at other values of liquid conductivity, e.g., at $\sigma = 90\,\text{Sm/m}$. No irregularities either appear in spatial distributions of absorption power across the liquid layer when increasing the
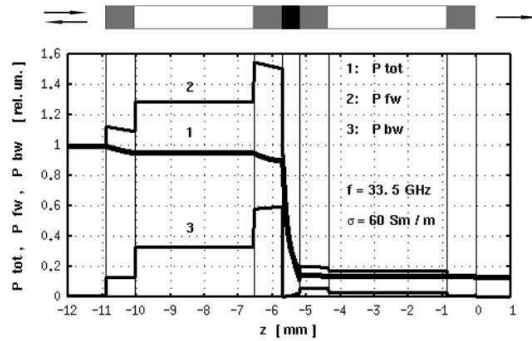
Figure 4. Total P_{tot}, forward P_{fw}, and backward P_{bw} mm-wave power fluxes (curves 1, 2 and 3, respectively) in the cell of Figure 1 at the frequency $f = 33.5\,\text{GHz}$ close to the first branch-point frequency $f_{01} = 33.00\,\text{GHz}$ when $\sigma = 60\,\text{Sm/m}$.
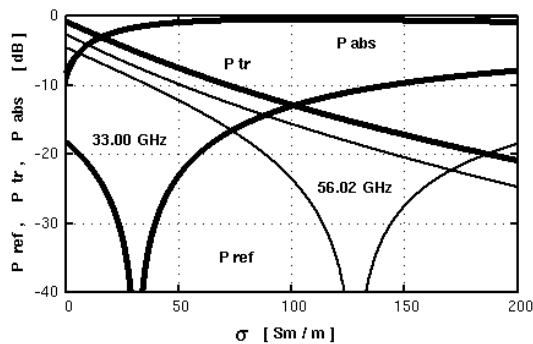
Figure 5. Reflection P_{ref}, transmission P_{tr}, and absorption P_{abs} power fluxes in the cell of Figure 1 computed as functions of liquid conductivity σ at the branch-point reflection notch frequencies $f_{01} = 33.00\,\text{GHz}$ and $f_{02} = 56.02\,\text{GHz}$.

frequency from below the first notch frequency f_{01} to the values exceeding the second notch frequency f_{02}.

5. PHASE BRANCH POINTS OF S_{11} AS REFLECTION NOTCH MARKERS

In addition to spatial distributions of power fluxes across the cell, we computed the total reflection, transmission and absorption power as functions of liquid conductivity σ precisely at the branch-point reflection notch frequencies f_{01} and f_{02} (Figure 5). The plot shows no features in transmission and absorption as functions of liquid conductivity, though it reveals very deep drops of reflection at certain values of σ specific for each notch frequency.

For a more complete picture, we plotted the magnitude of reflection power P_{ref} and the phase of reflected wave Φ_{ref} as functions

(a)

(b)
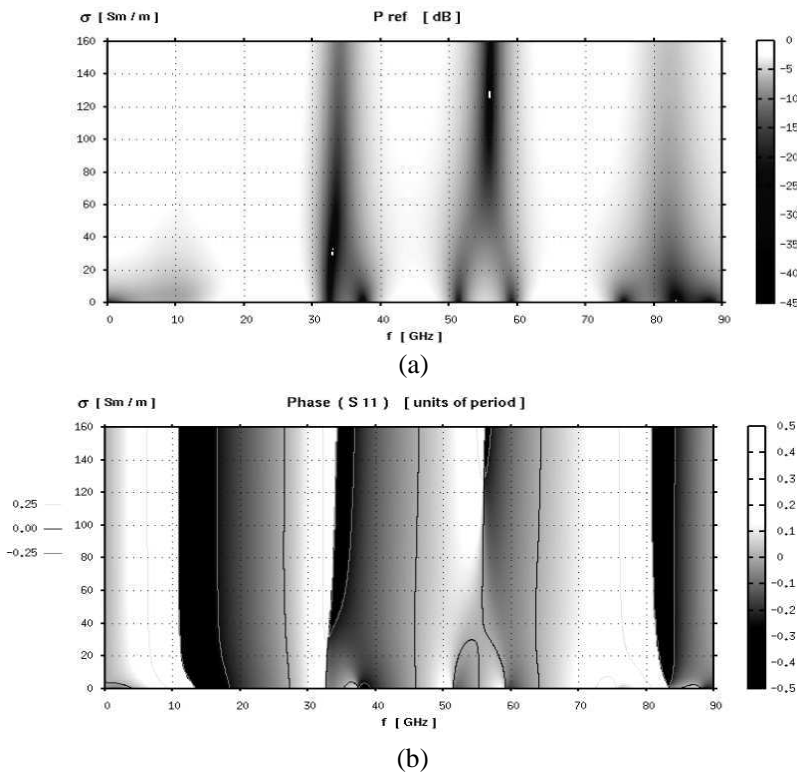
Figure 6. (a) Power P_{ref} and (b) phase Φ_{ref} of reflected wave as a function of frequency f and conductivity σ of liquid layer in the cell of Figure 1.

of both the frequency and liquid conductivity (Figure 6). The plots show that minima of reflection power correspond to branch points of phase function. So, branch points could be used as convenient markers of absolute reflection minima that occur at specific resonant values of frequency f_{0n} and liquid conductivity σ_{0n} (branch-point values).

Notice, the existence of branch points of phase function $\Phi_{ref}(f, \sigma)$ indicates that the reflection power drops to exact zero at these points presuming the ideal case of coherent monochromatic plane-wave excitation (real minima are of non-zero magnitude because of imperfections that create incoherent components, e.g., due to finite beam width and non-zero bandwidth of incident radiation). Both the transmission and absorption reveal broad maxima near the branch points, each at a slightly different frequency and of slightly different shape, but they are of such a kind that their sum makes very sharp peaks precisely at the branch points so as to satisfy the fundamental identity $P_{ref} + P_{tr} + P_{abs} = 1$.

6. PHASE TUNING IN BACK-REFLECTED WAVES AS A MECHANISM OF NOTCH FORMATION

All the facts presented above indicate that the formation of high-Q reflection notches cannot be explained by mere resonant absorption (e.g., no anomaly in absorption is seen in Figure 5 despite a significant drop of reflection being observed). Instead, the actual mechanism of notch formation could be understood as a result of phase tuning in back-reflected waves accompanied by power tuning that happens because of frequency and conductivity dependence of real and imaginary parts of refraction index of absorbing material (a liquid layer).

Since the complex refraction index is defined as $n = n_r + in_i = \sqrt{\epsilon}$, complex permittivity could be written as $\epsilon = \epsilon_r + i\epsilon_i = (n_r^2 - n_i^2) + 2in_r n_i$. This makes it clear that, once ϵ_i increases with increasing the conductivity and ϵ_r is set to be constant, the real part of refraction index $n_r = \mathrm{Re}\{n\}$ depends on conductivity along with imaginary part $n_i = \mathrm{Im}\{n\}$. This alters the phase relationships in reflected waves, in addition to variations in their amplitudes, when the waves propagate through the cell at different values of conductivity of a liquid layer. Then, at a certain combination of both the frequency and (non-zero) conductivity values, this would create the conditions for the exact cancellation of resulting back-reflected wave due to destructive interference of partial waves with properly adjusted phases and amplitudes, just as it happens in common anti-reflection coating structures.

Notice, the effect takes place in the presence of resonant absorption, though much more important fact is that the precise phase and power tuning occurs at finite (non-zero) conductivity of absorbing material.

To show that variations of both the real and imaginary parts of refraction index are playing a role in the notch formation, we consider two special cases. In the first case, we assume the actual frequency and conductivity dependence of imaginary part $n_i(f, \sigma) = \text{Im}\{n(f, \sigma)\}$ but accept the real part to be constant at either $n_{r1} = \text{Re}\{n(f_{01}, \sigma_{01})\}$ or $n_{r2} = \text{Re}\{n(f_{02}, \sigma_{02})\}$. In the second case, on the contrary, we assume the actual dependence of real part $n_r(f, \sigma) = \text{Re}\{n(f, \sigma)\}$ but accept the imaginary part as being constant at either $n_{i1} = \text{Im}\{n(f_{01}, \sigma_{01})\}$ or $n_{i2} = \text{Im}\{n(f_{02}, \sigma_{02})\}$.

Figure 7 shows the phase of reflected wave $\Phi_{ref}(f, \sigma)$ computed in

(a)

(b)
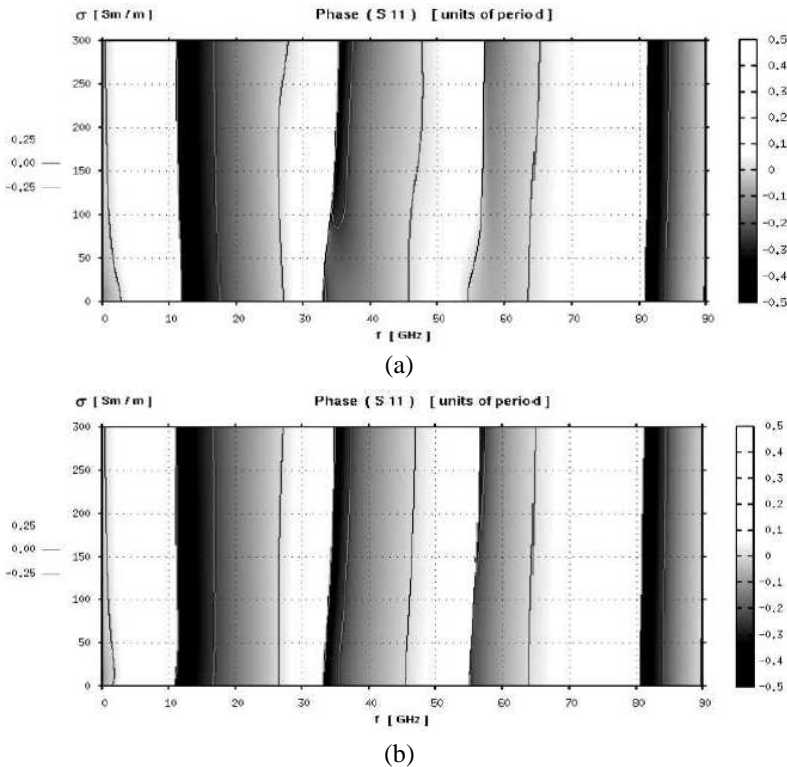
Figure 7. Phase of reflected wave Φ_{ref} as found by assuming the actual values of $n_r(f, \sigma)$ but accepting (a) $n_i = \text{Im}\{n(f_{01}, \sigma_{01})\}$ at $f_{01} = 33.00\,\text{GHz}$, $\sigma_{01} = 31.1\,\text{Sm/m}$ and (b) $n_i = \text{Im}\{n(f_{02}, \sigma_{02})\}$ at $f_{02} = 56.02\,\text{GHz}$, $\sigma_{02} = 128\,\text{Sm/m}$.

the second case when the only function of f and σ is the real part of refraction index $n_r(f, \sigma)$. Here, if the imaginary part is $n_i = n_{i1}$, twin branch points emerge near the former first reflection notch frequency (they are the only branch points to appear in this case) whereas, if $n_i = n_{i2}$, a single branch point near the former second notch frequency is only observed (the first branch point descends on the frequency axis). The branch points correspond to the conditions of exact canceling out of partial reflected waves when, in addition to counter-phase tuning, wave amplitudes are also adjusted due to absorption that occurs at the given imaginary parts of refraction index.

The effects in the case of $n_i(f, \sigma)$ at fixed $n_r = n_{r1}$ or n_{r2} look similar except that both the branch points at f_{01} and f_{02} appear at any of two values of n_r.

7. OPTIMIZATION OF THE MEASUREMENT CELL

Understanding the effect of sharpening the reflection notch with increasing the dielectric losses of absorbing substance in a stack resonator allows one to explain a similar effect in a capillary placed in a waveguide and, as a next step, to optimize the system so as to make it more accurate, sensitive, universal, and suitable for dielectric measurements of a broad range of liquid and solid materials.

The system of a capillary in a waveguide is qualitatively similar to the resonant stack, since a dielectric insertion in a waveguide creates an effective cavity around the insertion because of increasing the effective cross-section of the waveguide due to dielectric medium of permittivity $\epsilon_r > 1$. So, the effective cavity around the capillary behaves like the outer pair of plates in the stack resonator whereas the capillary walls operate as the inner plates.

If the parameters of both the capillary and the waveguide are chosen properly, a transmission notch appears (or, under other conditions, possibly, a reflection notch that was not noticed so far) just at the right frequency and conductivity as required. Yet, there is a limited flexibility in operation of capillary system, since the effective cavity parameters are tightly linked to capillary parameters, thus, restricting the variations of each parameter separately (unless we design a special waveguide cavity to remove the restrictions).

With a stack resonator, essential extensions of capabilities of the measurement system could be achieved. Figure 8 shows an example of increasing the range of conductivity values that could be measured with a cell of Figure 1 when air slots are chosen to be $a = 11.0\,\text{mm}$. Here we consider the model case of a water solution as a test liquid of permittivity $\epsilon(\omega)$ evaluated as complex permittivity of pure water
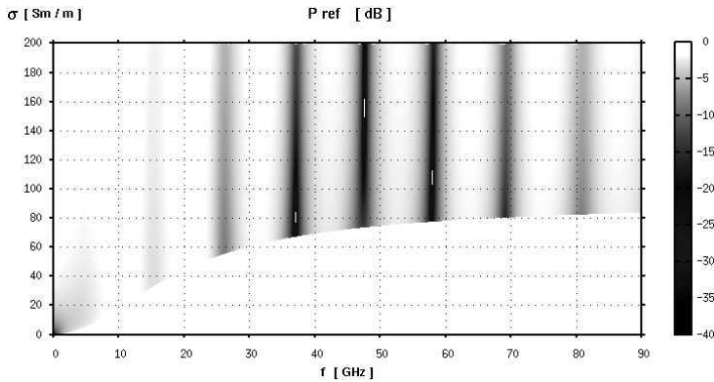
Figure 8. Power P_{ref} of reflected wave as a function of frequency f and conductivity σ of a test water solution in the cell of Figure 1 with air slots $a = 11.0$ mm (the bottom edge of the computed domain corresponds to $\sigma(\omega)$ of pure water).

$\epsilon_w(\omega)$ [18, 19] with additional conductivity σ_{add}. In this case, we assume, as an approximation, $\epsilon(\omega) = \epsilon_w(\omega) + i\sigma_{add}/\omega\epsilon_0$ so as the effective total conductivity is evaluated as $\sigma(\omega) = \omega\epsilon_0\text{Im}\epsilon(\omega)$ (Figure 8 appears to be remarkably similar to the one computed for the model liquid considered earlier). As one can see, the increase of air slots allows one to increase the values of conductivity that could be measured, and to reduce the frequency band where a few notch points are located.

Notice, unambiguous measurements require a set of data to be taken at a few reflection notch frequencies. Then, by comparing the reflection power measured at different frequencies, one can distinguish the cases when the same reflection at a certain notch frequency arises due to different values of σ (i.e., below and above the branch-point critical value that corresponds to the given reflection notch). In this way, one can measure the conductivity exceeding the critical value observed in the given frequency band (e.g., $\sigma > 200$ Sm/m in Figure 8).

Another improvement is the use of asymmetric cells that may have one size of air slots on the one side and another size on the other side (e.g., $a = 3.5$ mm on the left-hand side and $a = 11.0$ mm on the right-hand side). Since the reflection spectra are formed, mainly, in the front part of the cell (particularly, in the cells with heavily absorbing inner layers), specific patterns of the notch points of asymmetric cells are defined by the front side parameters. So, when illuminating different sides of asymmetric cell, one can measure with enhanced accuracy either the higher or the lower values of conductivity (or cross-check the results) of heavily absorbing inner layer, depending on situation.
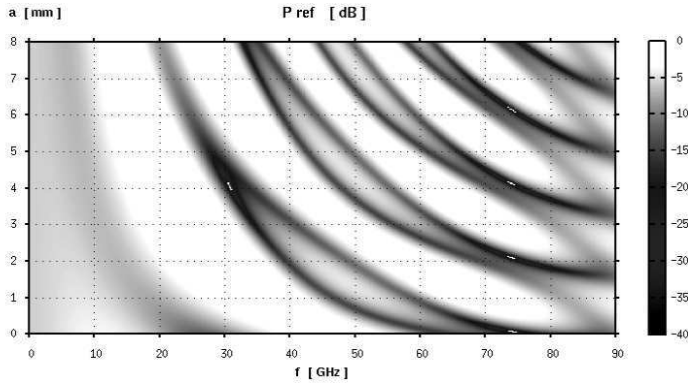
Figure 9. Power P_{ref} of reflected wave as a function of frequency f and air slots a in the cell of Figure 1 for measuring low conductivity of a model liquid (the plot shows the locations of minima of P_{ref} computed at $\sigma = 10\,\text{Sm/m}$).

Further possibilities arise when using stacks of other materials, multi-layer stacks in free space or similar kinds of stacks mounted in a waveguide, with or without a capillary as an additional element of a resonator, and with another size of air slots that should be adjusted for the waveguide mode propagation.

Finally, one may set the problem of optimizing the measurement cell for the particular range of frequency and conductivity values of a given layer of liquid or solid material. Figure 9 presents an example of optimization of air slots in the cell of Figure 1 intended for measuring low conductivity of a model liquid when the conductivity is expected to be about or below $\sigma = 10$ Sm/m. The plot shows the locations of minima of $P_{ref}(f, a)$ when computed assuming $\sigma = 10\,\text{Sm/m}$. The results indicate that, when using air slots $a = 4.0\,\text{mm}$, one would obtain the reflection notch points suitable for conductivity measurements at the frequencies $f = 30\,\text{GHz}$ and $f = 73\,\text{GHz}$.

8. CONCLUSIONS

Analysis and simulations of a one-dimensional stack (Bragg) dielectric-plate resonator have shown a possibility of using it for the measurement of high dielectric losses in the materials by means of a high-Q reflection notch method. The analysis provided an explanation of relevant effects concerning the reflection notch appearance and characteristic features.

The effect of sharpening the reflection notch in the frequency spectrum of millimeter waves with increasing the dielectric losses

(electric conductivity) of a slab or a cuvette with lossy liquid in a stack resonator is explained by counter-phase tuning of partial waves reflected from the slab (the cuvette) and from the other parts of resonator when the wave amplitudes are also adjusted in the process of resonant absorption.

Use of a few notch frequencies (preferably, in a broad frequency range) is needed for an unambiguous measurement of complex dielectric constant of the material (both its real and imaginary parts, i.e., both the index of refraction and the electric conductivity).

Asymmetric structures (e.g., those with different Bragg reflectors attached to the opposite sides of the slab or cuvette) are shown to provide additional benefits for expanding the domain of parameters being measured (e.g., for increasing the range of conductivity values).

More complicated structures based on the given effect could also be developed for further expanding the range of parameters and materials suitable for the investigation by the method.

ACKNOWLEDGMENT

REFERENCES

1. Clarke, R. N., A. P. Gregory, D. Cannell, M. Patrick, S. Wylie, I. Youngs, and G. Hill, *A Guide to the Characterisation of Dielectric Materials at RF and Microwave Frequencies*, NPL, Teddington, 2003.

2. Baker-Jarvis, J., M. D. Janezic, B. F. Riddle, R. T. Johnk, P. Kabos, C. L. Holloway, R. G. Geyer, and C. A. Grosvenor, *Measuring the Permittivity and Permiability of Lossy Materials: Solids, Liquids, Metals, Building Materials, and Negative-Index Materials*, NIST, Boulder, CO, 2005.

3. Afsar, M. N., N. Suwanvisan, and Y. Wang, "Permittivity measurement of low and high loss liquids in the frequency range of 8 to 40 GHz using waveguide transmission line technique," *Microw. Opt. Tech. Lett.*, Vol. 48, No. 2, 275–281, Feb. 2006.

4. Krupka, J., "Frequency domain complex permittivity measurements at microwave frequencies," *Meas. Sci. Technol.*, Vol. 17, No. 6, R55–R70, Jun. 2006.

5. Sheen, J., "Comparisons of microwave dielectric property measurements by transmission/reflection techniques and resonance techniques," *Meas. Sci. Technol.*, Vol. 20, No. 4, 042001, 2009.

6. Egorov, V. N., "Resonance methods for microwave studies of dielectrics (review)," *Instrum. Exp. Tech.*, Vol. 50, No. 2, 143–175, Mar. 2007.

7. Akay, M. F., Y. V. Prokopenko, and S. Kharkovsky, "Resonance characteristics of whispering gallery modes in parallel-plates-type cylindrical dielectric resonators," *Microw. Opt. Tech. Lett.*, Vol. 40, No. 2, 96–101, Jan. 2004.

8. Krupnov, A. F., V. N. Markov, G. Y. Golubyatnikov, I. I. Leonov, Y. N. Konoplev, and V. V. Parshin, "Ultra-low absorption measurement in dielectrics in millimeter- and submillimeter-wave range," *IEEE Trans. Microw. Theory Tech.*, Vol. 47, No. 3, 284–289, Mar. 1999.

9. Addamo, G., G. Virone, D. Vaccaneo, R. Tascone, O. A. Peverini, and R. Orta, "An adaptive cavity setup for accurate measurements of complex dielectric permittivity," *Progress In Electromagnetics Research*, Vol. 105, 141–155, 2010.

10. Chen, Q., K.-M. Huang, X. Yang, M. Luo, and H. Zhu, "An artificial nerve network realization in the measurement of material permittivity," *Progress In Electromagnetics Research*, Vol. 116, 347–361, 2011.

11. Matvejev, V., C. de Tandt, W. Ranson, J. Stiens, R. Vounckx, and D. Mangelings, "Integrated waveguide structure for highly sensitive THz spectroscopy of nano-liter liquids in capillary tubes," *Progress In Electromagnetics Research*, Vol. 121, 89–101, 2011.

12. Belyakov, E. V., "High-quality resonance in a waveguide with a highly-absorbing dielectric," *Elektronnaya Tekhnika. Ser. Elektronika SVCh (Electronic Engineering)*, Vol. 393, No. 9, 3–5, 1986.

13. Bakaushina, G. F., E. V. Belyakov, N. B. Zinov'eva, and A. M. Khrapko, "UHF-analyzer of concentration of liquid pharmaceutical substances," *Elektronnaya Tekhnika. Ser. Elektronika SVCh (Electronic Engineering)*, Vol. 393, No. 9, 54–56, 1986.

14. Belyakov, E. V., "A resonant UHF dielcometer for absorbing liquids," *Elektronnaya Tekhnika. Ser. Elektronika SVCh (Electronic Engineering)*, Vol. 401, No. 7, 51–53, 1987.

15. Belyakov, E. V., "Tunable UHF-resonator for measuring absorbing liquids," *Elektronnaya Tekhnika. Ser. Elektronika SVCh (Electronic Engineering)*, Vol. 424, No. 10, 59–61, 1989.

16. Kirichenko, A. Y., V. I. Lutsenko, Y. F. Filippov, Y. V. Prokopenko, and E. V. Krivenko, "Temperature-dielectric spectroscopy of aqueous solutions using the method of capillary-waveguide resonance," *Izv. VUZov. Radiofizika*, Vol. 51, No. 8, 711–716, 2008.

17. Bludov, Y. V., "Propagation of the H_{10} mode in a rectangular waveguide with a dielectric discontinuity," *Tech. Phys.*, Vol. 50, No. 8, 1062–1068, 2005.

18. Malyshenko, Y. I., V. L. Kostina, and A. N. Roenko, "A model of water dielectric permittivity in microwave and terahertz ranges," *Ukr. J. Phys.*, Vol. 52, No. 2, 155–161, 2007.

19. Furashov, N. I., V. E. Dudin, and B. A. Sverdlov, "Study of the dielectric properties of water in the frequency band 75–120 GHz," *Izv. VUZov. Radiofizika*, Vol. 49, No. 6, 489–501, 2006.

20. Born, M. and E. Wolf, *Principles of Optics*, 7th edition, Cambridge, 2003.